ACCEPTED MANUSCRIPT • OPEN ACCESS

Empirical evidence for multidecadal scale global atmospheric electric circuit modulation by the El Niño-southern oscillation

Empirical evidence for multidecadal scale Global Atmospheric Electric Circuit modulation by the El Niño-Southern Oscillation

R. Giles Harrison[a], Keri A. Nicoll[a], Manoj Joshi[b], Ed Hawkins[c]

[a]Department of Meteorology, Earley Gate, University of Reading, Reading. RG6 6ET UK

[b] Climatic Research Unit, School of Environmental Sciences, University of East Anglia. Norwich, Norfolk, NR4 7TJ, UK

[c]National Centre for Atmospheric Science, Department of Meteorology, University of Reading.

Abstract

The El Niño-Southern Oscillation (ENSO) modifies precipitation patterns across the planet. Charge separation in disturbed weather and thunderstorms drives the Global atmospheric Electric Circuit (GEC), hence ENSO-induced precipitation changes are anticipated to affect the global circuit. By analysing historical atmospheric electricity data using a new data processing procedure based on the Carnegie curve, signals correlated with ENSO sea surface temperature (SST) anomalies are revealed. These demonstrate a persistent ENSO-GEC relationship for the majority of the twentieth century, in Potential Gradient (PG) data from Lerwick, Shetland and Watheroo, W. Australia. The recovered data is weighted towards the first half of the UTC day, giving a GEC sensitivity up to ~5 % °C^{-1} of SST anomaly in the Niño 3.4 and 4 regions of the Pacific Ocean. Transferring ENSO variability by electrical means represents an unexplored teleconnection, for example, through proposed GEC effects on stratiform cloud microphysics. The strong ENSO-GEC relationship also provides a quality test for historical atmospheric electricity data, and encourages their use in reducing SST reconstruction uncertainties.

Keywords: ENSO, atmospheric electricity, potential gradient, teleconnection

1. Introduction

The Global atmospheric Electric Circuit (GEC) is embedded in the atmospheric system, balancing charge separation in disturbed weather regions with a return current in fair weather regions (Wilson, 1929). Through the GEC, positive charge is transported to upper conductive parts of the atmosphere generating a global equipotential - the ionospheric potential – with current flow to the surface, also sustaining the fair weather electric field (figure 1a). The GEC's well-known diurnal cycle – the *Carnegie* curve – was originally found to be correlated with thunderstorm area (Whipple and Scrase, 1936) , fig 1b. As the GEC is driven by convective weather, principally thunderstorms and shower clouds, internal climate system variability is expected to yield associated variability in the GEC (Harrison, 2004), with effects since identified on several timescales (Lavigne et al., 2017). This also represents an electrical teleconnection, as current flow through stratiform clouds leads to weak droplet charging (Baumgaertner et al., 2014), with possible charge-induced microphysical effects (Tinsley, 2008).

1

One major mode of internal climate variability is the El Niño-Southern Oscillation (ENSO), conventionally monitored through sea surface temperature (SST) anomalies in specific regions of the Pacific ocean, and with which changes in lightning have been associated (e.g. Sátori and Zieger, 1999). In the first reported observations of ENSO modulation of the GEC, Harrison et al (2011) showed that the annual variation of the Potential Gradient (PG) recorded in December at Lerwick, Shetland, which results from the GEC current, was positively correlated with the Niño 3.4 region sea SST anomalies between 1968 and 1983. The positive relationship was statistically robust from 09 UTC to 16 UTC, with sampling weighted to the morning hours. Recent detailed GEC modelling has now explained and confirmed the Lerwick observations as due to ENSO modulation of current generators (Slyunyaev et al., 2021a). Their positive SST relationship from 09 UTC to 15 UTC is consistent with the Lerwick findings, but, outside this interval, the Lerwick sampling is insufficient to assess the modelled negative relationship from 18 UTC to 23 UTC. (See also SI section B).

Investigation of a continued ENSO effect on the GEC is pursued here using recently recovered PG datasets from the first half of the twentieth century, with, additionally, a new data processing method. The SST anomalies considered, e.g. from the Hadley Centre reconstruction, HadISST1 (Rayner et al., 2003), or ERSST (Huang et al., 2017), are principally from the Pacific Ocean Niño 3.4 region, which covers the dateline to the South American coast (5°N to 5°S, 170°W to 120°W), but also for the Niño 4 region (5°N-5°S, 160°E-150°W) for the central equatorial Pacific, to allow for different regional expressions of ENSO identified (Kao and Yu, 2009) .
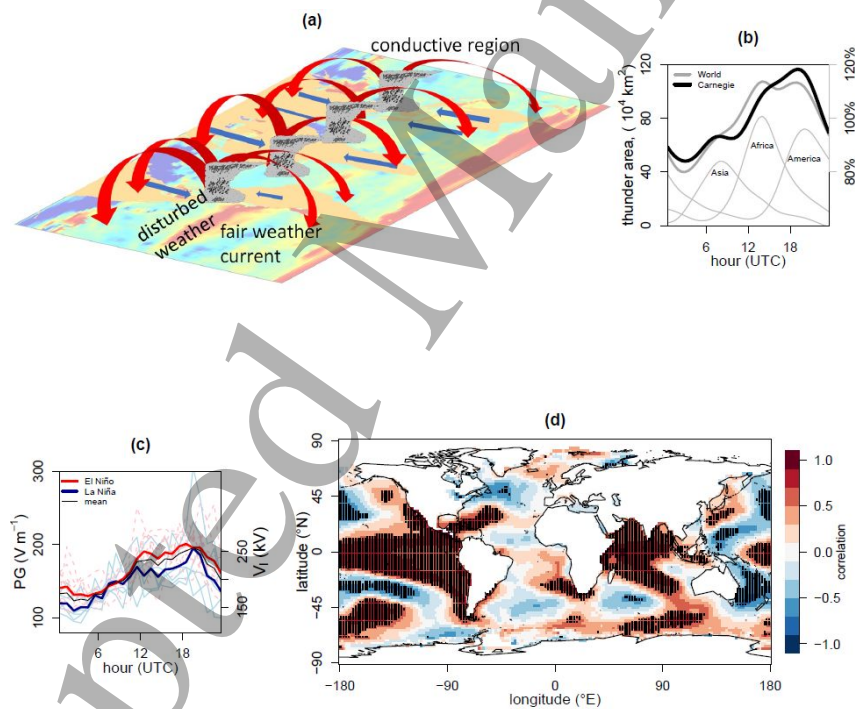
Fig1. (a) Schematic of the Global atmospheric Electric Circuit (GEC), in which charge separated in disturbed weather, such as equatorial thunderstorms, flows through the conductive upper atmosphere and to the surface in fair weather regions. (b) Measured GEC diurnal variation - the *Carnegie* curve (black line) – compared with land thunderstorm area (grey lines). (c) Mean annual diurnal PG at Lerwick during Decembers, 1968-1983 (individual El Niño and La Niña years dashed pink and light blue respectively, with associated mean values red and blue). (RHS vertical axis shows estimated upper atmosphere ("ionospheric") potential, V_I). (d) Spatial correlation between annual December Lerwick PG 1968-1983 and sea surface temperature anomalies (from ERSSTv5) in the same month. Stippling marks statistically significant correlations at the 95% level.

2.   ENSO effects in Lerwick PG data

The Carnegie curve (fig 1b) has a single maximum around 19 UTC and single minimum around 04 UTC (Harrison, 2013). Fig 1c demonstrates that the Lerwick Observatory PG data shows, on average, the same characteristic daily variation, and the GEC influence in the Lerwick PG data is also apparent from a close correlation with the ionospheric potential V_I (Harrison and Bennett, 2007). Fig 1c shows hourly mean Lerwick December PG values for each year, with El Niño and La Niña phases are separated, according to the Niño 3.4 SST anomaly being positive or negative respectively. From Harrison and Bennett(2007), the equivalent median ionospheric potential V_I changes from 188 kV (La Niña) to 214 kV (El Niño), i.e. an ENSO-induced V_I variation of ~20 kV.

Conventionally, the Carnegie curve is described by harmonic analysis, through amplitude and phase coefficients in

$$F(t) = A_0 + A_1 sin\left(\frac{t}{24}360° + \phi_1\right) + A_2 sin\left(\frac{2t}{24}360° + \phi_2\right) + A_3 sin\left(\frac{3t}{24}360° + \phi_3\right) + A_4 sin\left(\frac{4t}{24}360° + \phi_4\right) \qquad (1),$$

where F is the PG at time t (for t in hours UTC). A_0 represents the mean PG, and A_1 to A_4 amplitudes of the 24-hour, 12-hour, 8-hour and 6-hour harmonic contributions respectively, with ϕ_1 to ϕ_4 their associated phase angles (in degrees). Table 1 provides derived harmonic coefficients for the (relative) amplitude variations in the Lerwick PG in fig 1c, and the Carnegie curve. Changes are especially apparent in the 12-hour terms (A_2 and ϕ_2), likely to follow from contributions 12 hours out of phase with the usual maximum at 19 UTC, associated with disturbed weather in Asia.

Table 1. Harmonic coefficients derived from hourly mean values

	amplitude coefficients (%)					phase angles (°)				timing (UTC)	
	A_0	A_1	A_2	A_3	A_4	ϕ_1	ϕ_2	ϕ_3	ϕ_4	min	max
Carnegie 1928-9											
Nov-Dec-Jan	100	18.3	6.0	1.3	1.3	197.4	253.8	209.4	3.0	2.5	18.1
Dec	100	19.6	7.2	1.1	1.1	205.3	256.2	266.2	50.0	1.6	17.8
Lerwick 1968-1983 (Decembers)											
all	100	19.9	5.4	3.0	1.3	200.5	187.3	256.0	38.8	3.6	19.0
El Niño	100	20.5	3.6	3.0	1.3	197.1	171.2	251.3	68.5	4.3	18.6
La Niña	100	19.0	9.1	3.2	2.0	207.4	199.1	264.3	2.4	2.7	19.3

Further insight into the regional sources of GEC changes has been obtained by correlating the annual December PG at Lerwick (1968-1983) with the same years' December sea surface temperature anomalies, fig 1d. The major contributions are from tropical regions of the Pacific and Indian Oceans. (The relationship with tropical pressure is shown in Supp Info, SI, fig A1). Recent modelling results give additional context for varied spatial responses, as Slyunyaev et al. (2021c) found GEC contributions from land varied negatively with the Niño 3.4 index, and positively with Niño 3.4 over the oceans, with the net effect slightly positive. Further, comparisons with modelled shape variations in the daily (Carnegie) variation were made using PG data from Vostok, Antarctica between 2006 and 2016 (Slyunyaev et al., 2021b): similar changes are implied by Table 1, with the Lerwick daily PG maximum later for La Niña than El Niño.

As PG measurements were made globally throughout the twentieth century and indeed earlier, ENSO variations in other historical PG datasets are now investigated.

3. Global circuit data from the southern hemisphere

Although GEC observations can, in principle, be obtained anywhere, ocean measurements or pristine continental environments are preferred (Burns et al., 2017), as local effects on PG can otherwise dominate. Data processing strategies have been developed to reduce local influences and extract global circuit signals (e.g. Nicoll et al., 2019). Of these, identifying common variations across multiple sites, and seeking data under fair weather conditions (Harrison and Nicoll, 2018), can prove effective, either separately or in combination. Archive data sources may therefore have to be carefully processed to remove local influences, to recover underlying global circuit effects.

A particularly notable agreement between three distant atmospheric electricity monitoring sites was reported by Wait and Mauchly (1937). Consistent variations in annual PG data at Ebro (Spain), Huancayo (Peru) and Watheroo (Australia) were demonstrated, for averages across June-July-August-September (JJAS) between 1924 and 1935, using data originally classified as least disturbed.
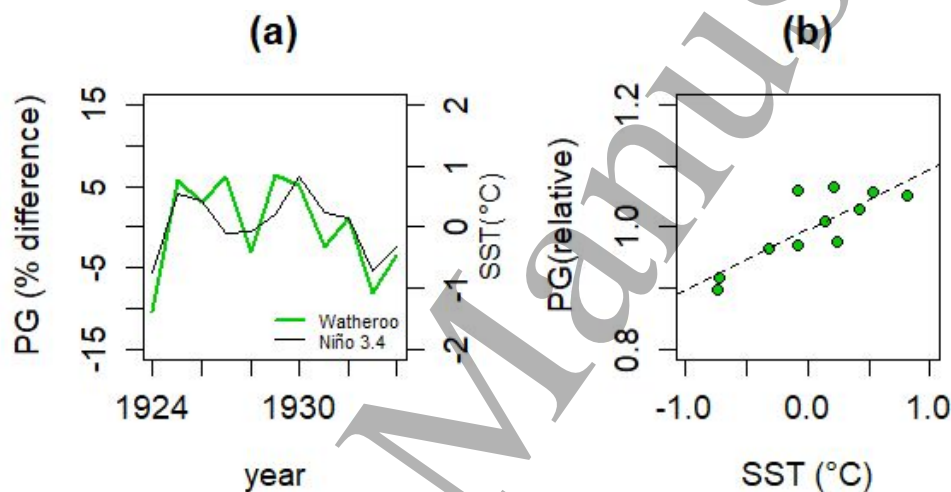

Fig 2. (a) PG time series from Watheroo (thick line), averaged annually for June-July-August-September (JJAS) from undisturbed days, as % differences from annual JJAS mean. Thin line shows simultaneous JJAS Niño 3.4 SST anomaly (from HadISST1). (b) Watheroo PG (relative values), plotted against JJAS Niño 3.4 SST anomaly. The probability p of the relationship in (b) arising by chance is p=0.006, allowing for persistence between years (Ebisuzaki, 1997).

Watheroo PG data from 1924 to 1934 are given in Carnegie Institution reports (Wait and Torreson, 1948), from which the calculated monthly averages have been transcribed. These were obtained on days originally selected for fair weather, to eliminate local effects such as bush burning by kangaroo hunters (Wait, 1943). Fig 2a shows annual PG values derived for JJAS, with the Niño 3.4 SST overplotted. Plotting Niño 3.4 SST against the average PG derived for these months shows a significant positive correlation, confirming a similar effect in the southern hemisphere winter to that observed in the northern hemisphere winter. The seasonality of the GEC itself is poorly known, limiting estimates of how the ENSO response might vary across the year.

The presence of the ENSO modulation in the southern hemisphere during the first half of the twentieth century encourages further investigation of the effect in northern hemisphere data in the same period.

4

4. Extension of the northern hemisphere Global Circuit data

Atmospheric electricity measurements began at Lerwick in 1924, with hourly values available from 1927 (Harrison and Riddick, 2022). This suggests a longer period of comparison with ENSO is possible than 1968-1983 considered in Harrison et al., 2011. The measurement apparatus used at Lerwick for the first half of the twentieth century was similar to the second half, but with a mechanical recording electrometer connected to a radioactive probe sensor.

This earlier Lerwick data cannot, however, be used directly between 1927 and 1967 for two reasons. Firstly, local radioactive contamination from weapons tests unfortunately compromised the measurement environment after about 1954, up to the mid-1960s (Hamilton and Paren, 1967). Secondly, the pre-contamination 1927-1954 measurements applied a different data selection process, using the overall character of each day's measurements. The 1968-1983 measurements previously analysed were instead selected meteorologically, for fair weather conditions. The modern fair weather method is not easily applied retrospectively, hence a new approach to remove local influences in the earlier data has been developed, now described.

(a) Earlier Lerwick PG data

Lerwick PG data from 1927-1954 have been recovered and digitised, again for each December following Harrison et al (2011). The values entered were restricted to least disturbed days, originally classified as "0a, 1a or 2a". This identified days on which the PG – usually positive in fair weather - was negative for less than three hours, with less than 1000 Vm^{-1} diurnal range.

Fig 3a shows the 1927-1954 December data for these days, plotted against UTC hour. Wide scatter is evident. For the 1927-1954 data, the inter-quartile range, IQR is 79 Vm^{-1}, compared with the 1968-1983 data (fig 1c), with an IQR of 50 Vm^{-1}. This is because the early "character" method of data classification would not have rejected electrically variable meteorological conditions, such as large PG values associated with fog. Nevertheless, the 1927-1954 values commonly lie around 100 Vm^{-1} and contain an underlying diurnal variation reminiscent of the Carnegie curve. Since the Carnegie curve varies by only about ±20 % around its mean daily value, values in fig 3a which lie well beyond this central range are unlikely to result from the GEC.

(b) Data selection

A method for removing outlier PG values is now investigated, based on assuming the standard Carnegie curve occurs every day and that observed PG values most likely to be associated with the global circuit will lie close to the standard Carnegie variation. Original data from the *Carnegie* itself has previously been reanalysed to determine the statistical range on the standard Carnegie curve variation (Harrison, 2013). Hourly PG values from Lerwick falling outside this typical range on the Carnegie curve are accordingly considered outliers. To preserve the largest number of Lerwick PG values potentially carrying a global circuit signal, values within three standard errors (σ) of each hourly mean value of the standard Carnegie curve are retained for further processing, broadly equivalent to selecting ~99 % of values possibly influenced by the global circuit. Fig 3b shows this range on the standard Carnegie curve for November-December-January, as a relative variation.
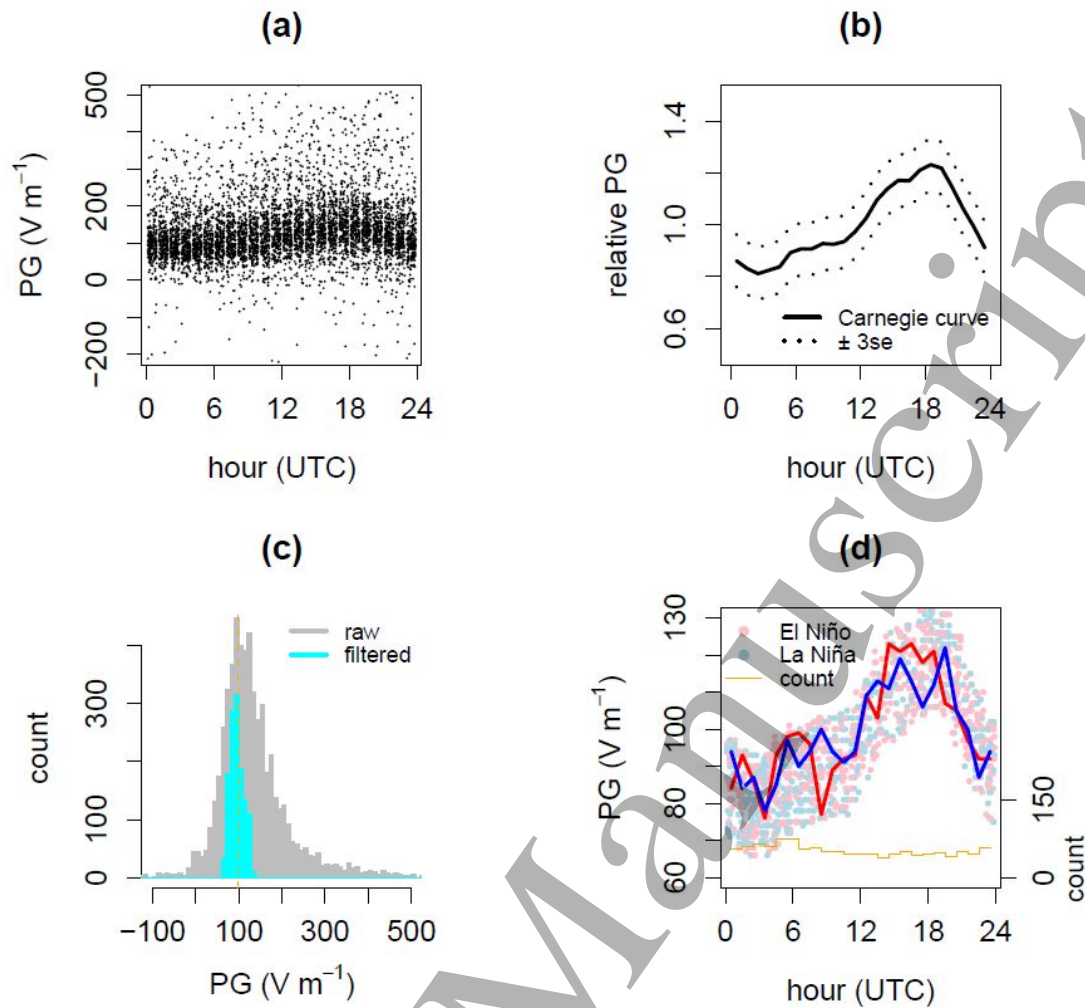
Fig 3. Filtering process used to select PG data. (a) Raw hourly PG values from Lerwick for Decembers 1927-1954, plotted against hour of day. (b) Carnegie curve (relative variations) for November-December-January (solid line), with a 3.0 standard error (se) range marked (dashed line).
(c) Distribution of raw Lerwick PG values from (a) (grey bars), with the distribution's mode marked with a dashed line. Inner (cyan) bars show filtered values remaining after the envelope in (b), normalised by the mode, was applied to the raw values of (a). (d) Filtered data plotted hourly, with points coloured during La Niña (light blue) and El Niño (pink) conditions and the associated hourly mode of the values (La Niña blue, and El Niño red), with number of hourly points retained given (orange line). In (a) and (d) small random horizontal jitter is used to reduce overplotting.

To apply the fig3b selection envelope to the fig 3a data, a representative central value for scaling the relative variation is needed. Fig 3c shows a histogram of the PG values from fig 3a, which has a long positive tail. Due to the asymmetry and tail of the distribution, the mean and median have larger values (133 Vm^{-1} and 120 Vm^{-1} respectively) than the mode (97 Vm^{-1}), hence the mode is chosen as the measure of central tendency. Fig 3c includes the revised distribution after applying the Carnegie curve selection envelope. This shows the removal of outliers beyond the specified range around the mode: the total number of data points is accordingly reduced, from 5664 to 1255 (22%), and the IQR becomes 22 Vm^{-1}. Hourly values remaining after the data selection are plotted in fig 3d, coloured by La Niña and El Niño circumstances: qualitatively, for 12 to 18 UTC, the mode of the El Niño values appears generally greater than for La Niña.

To assess the "Carnegie curve filter" further, Fig 4 compares median PG values for each December, before (fig 4a) and after (fig 4b) filtering. The range in each year is clearly reduced by the Carnegie filtering, with the number of values in each year's median falling by a factor of about five. For this data, the values retained tend towards early morning, 00 to 06 UTC (see also fig 3d).
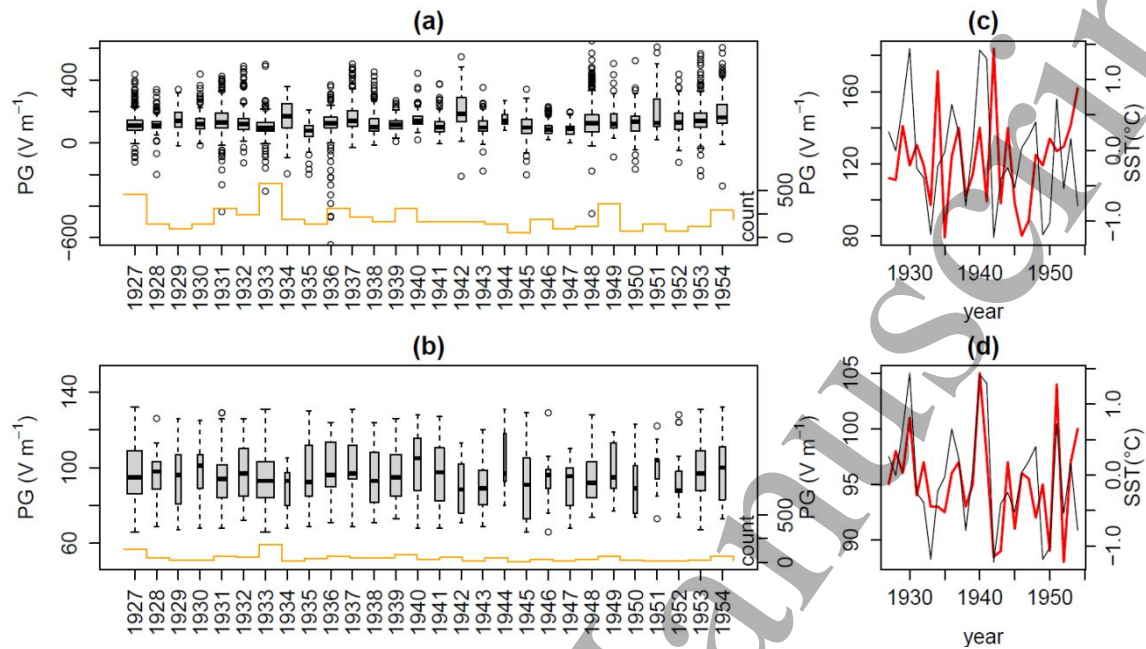

Fig 4. Comparison of yearly Lerwick December PG values (a) before and (b) after the filtering process, with the annual number of points retained (orange stepped line, RH-axis). (Box plots show medians, and inter-quartile range, box width proportional to the number of values). Right-hand column: Time series of mean yearly December PG (red line) and December Niño 3.4 region SST anomaly (from HadISST1), using (c) unfiltered (d) filtered PG data.

5.   Discussion

Informed by the Watheroo PG data, the earlier Lerwick dataset from a similar era is compared with the Niño 3.4 SST in figs 4c and fig 4d. For the original unfiltered data, there is little agreement (Spearman correlation coefficient r = -0.02). In the filtered data, however, there is much better agreement (r = 0.61), including for the strong Pacific 1940-2 event (Brönnimann et al., 2004). Evidently, the Carnegie filtering retains values more strongly associated with ENSO changes and rejects the much larger proportion of values probably affected by local factors. The original choice of 3σ for the data selection range was statistically informed, although arbitrary: in fact, the correlation between the filtered annual PG and Niño 3.4 index can be increased further using 2.8σ, yielding r = 0.63, retaining 21% of the original values. The specific choice is not particularly critical between 2.0σ and 4.0σ (see SI, section C). The same methodology was also applied to the Watheroo hourly data for July, during 1924 to 1934 (SI, section D), yielding values principally around 09-15UTC.

The three PG datasets from Watheroo and Lerwick (1927-1954, and 1968-1983) have been combined and plotted against SST for both the Niño 3.4 region and the central equatorial region, Niño 4, in fig 5, using monthly PG averages across all hours. The relationship with Niño 3.4 (fig 5a) shows more scatter than Niño 4 (fig 5b), but the sensitivity is greater with Niño 4. The agreement in

both cases indicates a GEC response to ENSO in the northern hemisphere in both the first and second parts of the twentieth century, and in the southern hemisphere during the first part of the twentieth century. With either Niño 3.4 or 4 SST anomalies (representing Eastern Pacific or Central Pacific based ENSO respectively), the earlier (1927-1954) and later (1968-1983) Lerwick data show statistically similar SST sensitivities, with the Watheroo (1924-1934) sensitivity slightly greater (Table 2), likely to be associated with different GEC behaviour in different seasons or different diurnal contributions. Statistical significance is also estimated, allowing for inter-year persistence (Ebisuzaki, 1997). A similar comparison with the Dipole Mode Index for the Indian Ocean did not yield statistically significant relationships, although this variability has been linked with African rainfall rather than the Pacific (Jiang et al., 2021).
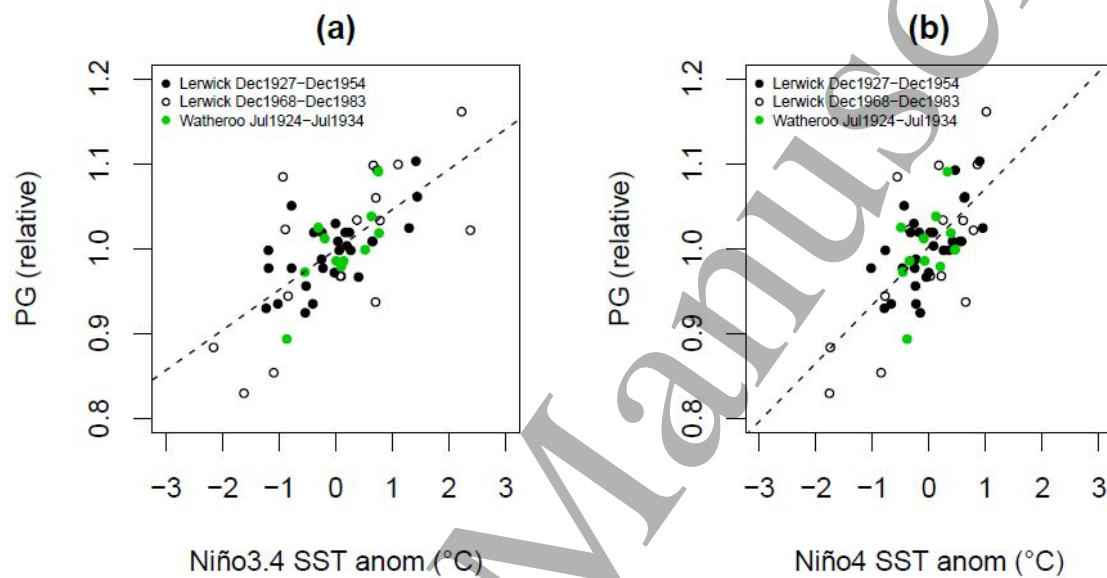

Fig 5. Variation of relative PG (normalised by the site's mean value over the interval), with (a) Niño 3.4 and (b) Niño 4 region SST anomaly (from HadISST1), for Watheroo (1924-1934, Carnegie filtered least disturbed days), Lerwick (1968-1983 fair weather values; 1927-1954, Carnegie filtered least disturbed days).

Table 2. Sensitivity of Global Circuit El Niño response with monthly mean values

Site	Period	Month (and principal contribution times)	Sensitivity (% °C^{-1}) (and standard error)	
			Niño 3.4	Niño 4
Watheroo	1924-1934	Jul (09-15UTC)	6.8 ± 2.0 ($p<0.01$)	6.6 ± 4.0 ($p<0.1$)
Lerwick	1927-1954	Dec (00-06UTC)	3.9 ±0.9 ($p<0.001$)	5.1 ± 1.4 ($p<0.003$)
Lerwick	1968-1983	Dec (09-18UTC)	5.2 ± 1.4 ($p<0.003$)	7.9 ± 1.9 ($p<0.001$)
all	**1924-1983**		**4.7 ± 0.7**	**6.9 ± 1.1**

Overall, the sensitivity from both hemispheres is 4.7% °C^{-1} of SST anomaly for Niño 3.4, or 6.9% °C^{-1} for Niño 4. Using the Extended Reconstructed Sea Surface Temperature (ERSST) version 5, the sensitivities are (4.1±0.7) % °C^{-1} and (5.5±1.1) % °C^{-1} respectively (see SI, fig D1). The agreement between the PG and SST anomalies adds confidence to the SST reconstructions. As a corollary, this

8

suggests that historical atmospheric electricity datasets can provide corroboration with SST datasets, in which uncertainties remain (Huang et al., 2016).

6. Conclusions

In summary, this analysis confirms a global circuit response to ENSO for the majority of the twentieth century. This reveals a new route by which ENSO variations are communicated throughout the atmosphere. It also provides further evidence for the operation of the global circuit as an embedded part of the climate system. From this, it follows that atmospheric electricity data can also implicitly contain climate information.

The ENSO-GEC modulation is sufficiently strong to allow SST data to be used as comparator against which to test PG data for GEC variations. Further, as ENSO indices are uncertain for some periods, and an effective method of processing historical PG data to extract the global circuit signals has been demonstrated, atmospheric electricity data can be considered more widely for corroborating and supporting SST reconstructions.

Conflict of Interest statement

The authors declare no conflict of interest.

Data availability

The data that support the findings of this study are openly available, at https://doi.org/10.17864/1947.000409 . The Pacific Ocean temperature anomalies were from https://climexp.knmi.nl/selectindex.cgi , data for fig 1b from Harrison, (2013), and for fig1d from NOAA/ESRL Physical Sciences Laboratory, Boulder, Colorado (http://psl.noaa.gov//).

References

Baumgaertner, A. J. G., Lucas, G. M., Thayer, J. P., and Mallios, S. A.: On the role of clouds in the fair weather part of the global electric circuit, Atmos. Chem. Phys., 14, https://doi.org/10.5194/acp-14-8599-2014, 2014.

Brönnimann, S., Luterbacher, J., Staehelin, J., Svendby, T. M., Hansen, G., and Svenoe, T.: Extreme climate of the global troposphere and stratosphere in 1940-42 related to El Niño, Nature, 431, 971–

974, https://doi.org/10.1038/nature02982, 2004.

Burns, G. B., Frank-Kamenetsky, A. V., Tinsley, B. A., French, W. J. R., Grigioni, P., Camporeale, G., and Bering, E. A.: Atmospheric global circuit variations from vostok and concordia electric field measurements, J. Atmos. Sci., 74, https://doi.org/10.1175/JAS-D-16-0159.1, 2017.

Chang, C. P., Wang, Z., Ju, J., and Li, T.: On the relationship between western maritime continent monsoon rainfall and ENSO during northern winter, J. Clim., 17, https://doi.org/10.1175/1520-0442(2004)017<0665:OTRBWM>2.0.CO;2, 2004.

Ebisuzaki, W.: A method to estimate the statistical significance of a correlation when the data are serially correlated, J. Clim., 10, https://doi.org/10.1175/1520-0442(1997)010<2147:AMTETS>2.0.CO;2, 1997.

Hamilton, R. A. and Paren, J. G.: The influence of radioactive fallout on the atmospheric potential gradient, Meteorol. Mag., 96, 81–85, 1967.

Harrison, R. G.: The global atmospheric electrical circuit and climate, Surv. Geophys., 25, https://doi.org/10.1007/s10712-004-5439-8, 2004.

Harrison, R. G.: The Carnegie curve, Surv. Geophys., 34, 209–232, https://doi.org/10.1007/s10712-012-9210-2, 2013.

Harrison, R. G. and Bennett, A. J.: Multi-station synthesis of early twentieth century surface atmospheric electricity measurements for upper tropospheric properties, Adv. Geosci., 13, https://doi.org/10.5194/adgeo-13-17-2007, 2007.

Harrison, R. G. and Nicoll, K. A.: Fair weather criteria for atmospheric electricity measurements, J. Atmos. Solar-Terrestrial Phys., 179, 239–250, https://doi.org/10.1016/j.jastp.2018.07.008, 2018.

Harrison, R. G. and Riddick, J. C.: Atmospheric electricity observations at Lerwick Geophysical Observatory, Hist. Geo Space. Sci, 13, 133–146, https://doi.org/10.5194/hgss-13-133-2022, 2022.

Harrison, R. G., Joshi, M., and Pascoe, K.: Inferring convective responses to El Niño with atmospheric electricity measurements at Shetland, Environ. Res. Lett., 6, https://doi.org/10.1088/1748-9326/6/4/044028, 2011.

Huang, B., L'Heureux, M., Hu, Z. Z., and Zhang, H. M.: Ranking the strongest ENSO events while incorporating SST uncertainty, Geophys. Res. Lett., 43, https://doi.org/10.1002/2016GL070888, 2016.

Huang, B., Thorne, P. W., Banzon, V. F., Boyer, T., Chepurin, G., Lawrimore, J. H., Menne, M. J., Smith, T. M., Vose, R. S., and Zhang, H. M.: Extended reconstructed Sea surface temperature, Version 5 (ERSSTv5): Upgrades, validations, and intercomparisons, J. Clim., 30, https://doi.org/10.1175/JCLI-D-16-0836.1, 2017.

Jiang, Y., Zhou, L., Roundy, P. E., Hua, W., and Raghavendra, A.: Increasing Influence of Indian Ocean Dipole on Precipitation Over Central Equatorial Africa, Geophys. Res. Lett., 48, https://doi.org/10.1029/2020GL092370, 2021.

Kalnay, E., Kanamitsu, M., Kistler, R., Collins, W., Deaven, D., Gandin, L., Iredell, M., Saha, S., White, G., Woollen, J., Zhu, Y., Chelliah, M., Ebisuzaki, W., Higgins, W., Janowiak, J., Mo, K. C., Ropelewski, C., Wang, J., Leetmaa, A., Reynolds, R., Jenne, R., and Joseph, D.: The NCEP/NCAR 40-year reanalysis project, Bull. Am. Meteorol. Soc., 77, https://doi.org/10.1175/1520-0477(1996)077<0437:TNYRP>2.0.CO;2, 1996.

Kao, H. Y. and Yu, J. Y.: Contrasting Eastern-Pacific and Central-Pacific types of ENSO, J. Clim., 22, https://doi.org/10.1175/2008JCLI2309.1, 2009.

Lavigne, T., Liu, C., Deierling, W., and Mach, D.: Relationship between the global electric circuit and electrified cloud parameters at diurnal, seasonal, and interannual timescales, J. Geophys. Res. Atmos., 122, https://doi.org/10.1002/2016JD026442, 2017.

Nicoll, K. A., Harrison, R. G., Barta, V., Bor, J., Brugge, R., Chillingarian, A., Chum, J., Georgoulias, A. K., Guha, A., Kourtidis, K., Kubicki, M., Mareev, E., Matthews, J., Mkrtchyan, H., Odzimek, A., Raulin, J.-P., Robert, D., Silva, H. G., Tacza, J., Yair, Y., and Yaniv, R.: A global atmospheric electricity monitoring network for climate and geophysical research, J. Atmos. Solar-Terrestrial Phys., 184, 18–29, https://doi.org/10.1016/j.jastp.2019.01.003, 2019.

R Core Team: R: A Language and Environment for Statistical Computing, 2021.

Rayner, N. A., Parker, D. E., Horton, E. B., Folland, C. K., Alexander, L. V., Rowell, D. P., Kent, E. C., and Kaplan, A.: Global analyses of sea surface temperature, sea ice, and night marine air temperature since the late nineteenth century, J. Geophys. Res. Atmos., 108, https://doi.org/10.1029/2002jd002670, 2003.

Sátori, G. and Zieger, B.: El Niño related meridional oscillation of global lightning activity, Geophys. Res. Lett., 26, https://doi.org/10.1029/1999GL900264, 1999.

Slyunyaev, N. N., Ilin, N. V., Mareev, E. A., and Price, C. G.: A new link between El Nino - Southern Oscillation and atmospheric electricity, Environ. Res. Lett., 16, https://doi.org/10.1088/1748-9326/abe908, 2021a.

Slyunyaev, N. N., Frank-Kamenetsky, A. V., Ilin, N. V., Sarafanov, F. G., Shatalina, M. V., Mareev, E. A., and Price, C. G.: Electric Field Measurements in the Antarctic Reveal Patterns Related to the El Niño—Southern Oscillation, Geophys. Res. Lett., 48, https://doi.org/10.1029/2021GL095389, 2021b.

Slyunyaev, N. N., Ilin, N. V., Mareev, E. A., and Price, C. G.: The global electric circuit land–ocean response to the El Niño—Southern Oscillation, Atmos. Res., 260, https://doi.org/10.1016/j.atmosres.2021.105626, 2021c.

Tinsley, B. A.: The global atmospheric electric circuit and its effects on cloud microphysics, https://doi.org/10.1088/0034-4885/71/6/066801, 2008.

Wait, G. R.: Effect of smoke on the atmospheric-electric elements at the Watheroo Magnetic Observatory, J. Geophys. Res., 48, https://doi.org/10.1029/te048i001p00049, 1943.

Wait, G. R. and Mauchly, J. W.: World-wide changes in potential gradient, Eos, Trans. Am. Geophys. Union, 18, https://doi.org/10.1029/TR018i001p00169, 1937.

Wait, G. R. and Torreson, O. W.: Atmospheric electric results from Watheroo Observatory, Western Australia, Carnegie Institution of Washington, 1948.

Whipple, F. J. W. and Scrase, F. J.: Point discharge in the electric field of the Earth, Geophys Mem Met Off L. , 11, 1–20, 1936.

Wilson, C. T. R.: Some thundercloud problems, J. Franklin Inst., 208, 1–12, https://doi.org/10.1016/S0016-0032(29)90935-2, 1929.